PIV Characterisation of Flocculation Dynamics and Floc Structure in Water Treatment

F. Xiao[a], K. M. Lam [a], X. Y. Li[a],* , R.S. Zhong[b] and X.H. Zhang[b]

[a] Environmental Engineering Research Centre, Department of Civil Engineering,
The University of Hong Kong, Pokfulam Road, Hong Kong, China
[b] Research Center for Environmental Engineering & Management, Graduate School at
Shenzhen, Tsinghua University, Shenzhen, China

*Corresponding Author:

Phone:	(852) 2859-2659
Fax:	(852) 2559-5337
Email:	xlia@hkucc.hku.hk
Homepage:	http://web.hku.hk/~xlia/

Running Head: Particle flocculation and coagulation, Water treatment

1 **Abstract**

2 Particle flocculation with chemical flocculant addition is an essential step in water treatment.

3 The performance of flocculation and the property of the flocs formed affect the overall results

4 of the treatment process. In addition to particulate impurities, the presence of organic matter

5 in water, such as natural organic materials (NOM), also influence the effectiveness of

6 chemical flocculation. In this paper, the PIV system was employed to investigate the

7 flocculation dynamics for different flocculants in different model waters. With the PIV and

8 image analysis, the change in particle size distribution could be well recorded. Using the

9 sequence of flocculation, shear breakage and re-flocculation on a jar-test device together with

10 the PIV system, the rate of floc formation, the strength of the flocs, the recovery of broken

11 flocs, and the morphological and structural features of the flocs were characterized. The

12 results indicated that the adsorption of HA on the particle will stabilized the particles, hence

13 hindered the flocculation process. Sweep flocculation using a higher chemical coagulant

14 dosage was an effective means of process enhancement for the removal of particulates and

15 associated organic matter. The dynamics of A-B-R process was characterized by particle size

16 distribution (PSD) measurement with PIV setup. The particle strength and reversibility

17 capability were examined. Strength index showed the HA flocs have comparable strength,

18 while recovery index indicated a less recovery capability with the increasing of HA

19 concentration after exposure to a higher shear, especially for ferric HA flocs. It appears that

20 the bonds holding HA flocs together are not purely physical bonds given the limited regrowth

21 seen. Finally, evolution of floc structure during A-B-R process was analyzed by investigated

22 the fractal dimension D_b. The results were generally consistent with previous PSD

23 measurements. It suggested that the structure of flocs in breakage became more compact with

24 little permeability. An increase in floc compaction provides a further explanation for the

25 limited regrowth for most of flocs. According to the performances of alum and ferric, it can

26 be noticed that HA flocs have different properties dependent on which chemical coagulant is

27 used. Alum produced larger HA flocs which endured a higher recovery capability after

28 exploring higher shear, hence, compared to ferric, it could be preferred to using in the

29 practical enhanced coagulation unit.

30

31 *Keywords:* Aggregation-breakage-re-flocculation; humic acid; hydrodynamics; particle image

32 velocimetry (PIV).

33

1. Introduction

Humic acids (HAs) are one of the main constitute of natural organic matter (NOM) in most water sources, resulting from the weathering and biodegradation of dead plants and animals [1, 2]. The presence of NOM in the water is a major concern not only to form the disinfection by-products, such as trihalomethanes (THMs), but to reduce the effectiveness of filtration processes, such as membrane fouling [3, 4]. Since United States Environmental Protection Agency has proposed that enhanced coagulation is a best available technology for NOM removal [5, 6], extensive studies are addressed on the performance of humic acid coagulation [7-9], however little thought is given to the physiochemical characteristics of HA flocs. It includes floc size, compaction, strength and the potential to regrow after being broken.

Enhanced coagulation is still a shear-induced flocculation, which means the shear flow is a main reason to result in collisions which cause the flocs to grow. However, they can still be subjected to higher shear rates where the flocs have to resist the corresponding stresses [10]. By use of model spherical particles, such as latex beads, it has been previously shown that particle suspensions destabilized with an ionic salt (i.e. NaCl) will reform to their initial size if the original velocity gradient is subsequently reapplied [11]. This behaviour is known as reversible breakage. However, in most instances where conventional metal coagulants and polymers are used for the aggregation of small particle suspensions (such as precipitated solids), irreversible breakage is usually seen, such that the initial floc size is never subsequently achieved after breakage.

The irreversibility of aggregates during cycled shear is most likely the result of particle-flocculant bond breakage during fragmentation, hence the reorganisation and restructuring can both occur. Experimental shear-induced coagulation-fragmentation processes [11-14] found that the fractal dimension shifts to a larger value compared to the

59   initial one, which showed a more compact structure formed during the cycled shear.

60   However, there has been no previous work showing the regrowth potential of HA flocs with

61   different coagulants and the structure restructuring and reorganisation during a cycled shear

62   schedule. Thus, an understanding of the reversible potential for natural organic flocs may

63   provide an important addition to the well-studied field of HA enhanced flocculation.

64   The structure of the HA containing flocs is non-homogeneous and should be

65   described by the fractal scaling law [15-17]. This fractal structure would affect the properties

66   of the flocs during aggregation-breakage-regrowth process. Although, more research effort

67   has been made to specify the properties of HA containing flocs, there is no study to report the

68   exact influence of the fractal structure on the hydrodynamic behaviours of flocs formed in

69   water treatment. Therefore, it merits more efforts to investigate the hydrodynamic properties

70   of the HA containing flocs and their relationship with the fractal structure of the flocs.

71   In present work, a series of the standard jar-tests were carried out to predict the

72   overall result of water flocculation and sedimentation. ζ-potential, turbidity removal and HA

73   reduction were determined for the particle suspension at various coagulant dosage. An

74   improved experimental facility for characterization of the PSD dynamics was developed by

75   making use of particle image velocimetry (PIV) coupled with image-analysis system. This

76   non-intrusive measurement of PSD was performed to characterize the HA flocs during

77   aggregation-breakage-regrowth (A-B-R) process. Morphology evolution indicated by surface

78   fractal dimension, breakage and regrowth potential of different HA flocs were evaluated with

79   different coagulants.

80

81   **2. Materials and Methods**

82

83   *2.1 Model waters and jar-test flocculation experiments*

5

84   Humic acid (HA) (Florida peat humic acid reference: 1R103H-2) was obtained from

85   International Humic Substances Society, and the stock HA solution was made by dissolving

86   the HA into de-ionized water. Kaolin (Aldrich, Milwaukee, WI) with a mean size of around

87   2.6 μm was used for making particle suspensions. Three types of the model waters that

88   contained 10 mg/L kaolin with an initial turbidity of 12 NTU and different HA contents were

89   prepared for the experimental study, including (1) HA0 – no HA addition, (2) HA3 - 3 mg/L

90   HA in water measured in terms of dissolved organic carbon (DOC), and (3) HA10 - 10 mg

91   DOC/L of HA. Two flocculants – alum ($Al_2(SO_4)_3 \cdot 14H_2O$) (BDH Chemicals, England) and

92   ferric chloride ($FeCl_3 \cdot 6H_2O$) (UNI-Chem, Mumbai, India) - were tested for the flocculation

93   performance.

94   Standard jar-test flocculation and sedimentation experiments were conducted at room

95   temperature (~22 °C) the model waters with a jar-test device (ZR4-6, Zhongrun, Shenzhen,

96   China). The jar-tester consisted of six 1-L rectangular beakers, each was filled with 500 mL

97   water, and the mixing was provided by with flat paddle mixers (5.0×4.0 cm^2). For each

98   model water, a flocculant, alum or ferric, was added at various dosages from 0 to 50 mg/L

99   into the six beakers. Throughout a flocculation experiment, the water pH was monitored by a

100   pH meter (420A, Orion, Boston, MA). 1 M $NaHCO_3$ was used to adjust the solution pH to a

101   proper range for the different flocculant dosages, i.e. pH~7.0 for alum flocculation and

102   pH~6.5 for ferric flocculation.

103   For a jar-test run, the water after the chemical addition was mixed rapidly at 100 rpm

104   for 60 sec. A sample of 10 mL was then withdrawn from each beaker for particle ζ-potential

105   measurement by a laser ζ-potential analyzer (Delsa 440SX, Coulter, Amherst, MA).

106   Following the rapid mixing, the water in the jar-test beakers was mixed for flocculation at a

107   slower rate of 30 rpm for 40 min followed by 30 min of sedimentation. The supernatant was

108   collected, for which the turbidity and HA residues were analyzed. The turbidity was

109   measured with a Turbidimeter (2100N, HACH, Loveland, CO), and the DOC in water was

110   measured by a TOC analyzer (5000A, Shimadzu, Kyoto, Japan). In addition, based on the ζ-

111   potential measurement and jar-test results, the optimal dose of a flocculant for a model water

112   could be determined. The optimal dose was then used for the flocculation-breakage-

113   reflocculation experiment on the model water characterized by the PIV technique.

114

115   *2.2 Particle image velocimetry (PIV) for particle size distribution measurement*

116   A PIV system was employed to track the change in particle size distribution (PSD)

117   during a flocculation experiment. PIV is an advanced and powerful flow visualization and

118   particle tracking technique [18]. As a non-intrusive optical setup, the PIV was able to capture

119   the image of particles in a jar-test beaker within a millisecond (Figure 1). The PIV system

120   consists of a laser illumination setup, a high-speed CCD video camera and a process control

121   and image processing software package. A pulsed laser beam generated from the source

122   (Coherent, Inc., Santa Clara, USA) was expanded to a thin laser light sheet by a combination

123   of a cylindrical and a spherical lenses. The laser sheet illuminated a planar region of the water

124   for visualization of the particles and flocs in the flocculation tank (beaker). The images of

125   laser-illuminated particles could be captured by a high speed CCD camera (PCO.imaging

126   1200 with a resolution of 1280×1024 pixels). The PIV system was controlled by a computer

127   with dedicated software (PCO.camware) for laser flushing, CCD recording, image acquisition

128   and storage. Images were processed with an image analysis system (Scion Image, Frederick,

129   MD) for PSD determination. For a floc of irregular shape, its size, d, was calculated in terms

130   of the equivalent diameter by $d = (4A/\pi)^{1/2}$, where A is the projected area of the floc. Based on

131   calibration, the PIV system had a resolution of around 9 µm for particle tracking and imaging

132   in the present flocculation study. More than 40 consecutive images within a minute were

analyzed to produce a size distribution of the particles, and the result was presented as either a number-based discrete PSD or a volume-based discrete PSD.

In addition to size measurement, particle image analysis also can provide more information about the morphological and structural feature of the aggregate flocs. For the 2-D projected particle images, a boundary fractal dimension was used to characterize the fractal property of the flocs. The boundary fractal dimension defines how the projected areas of the particles scale up with the length of the perimeter [14, 16]. Accordingly, the boundary fractal dimension, D_b, may be determined from the correlation [16, 19] as follows,

$$A \propto P^{2/D_b} \tag{3}$$

where P is the perimeter of an aggregate. D_b ranges from 1 to 2, and there is no straightforward relationship between D_b and the mass fractal dimension for a particle population [15]. Nonetheless, a higher D_b value often suggests a more fractal structure of the objects with a less spherical shape and irregular or rough surface [16].

2.3 Flocculation-breakage and reflocculation test for floc strength and re-growth

A single beaker jar-test device was used together with the PIV for characterization of the flocculation dynamics (Figure 1). The jar-tester included a glass rectangular tank (L×W×H = 80 × 80 × 200 mm) equipped with a flat paddle mixer that was driven by a DC power supply. The flocculation procedure on a model water was the same as previous described, i.e., after the chemical addition a pre-determined dose, the water was stirred rapidly at 100 rpm for 60 s followed by a slow mixing at 30 rpm for 30 min. Upon the completion of flocculation, the shear breakage and then re-flocculation experiment was carried out. The breakage of flocs was conduced at 100 rpm for 15 min, which was followed by re-flocculation with slow mixing at 30 rpm for 30 min. During the course of flocculation-

157 breakage-reflocculation, the images of particles and flocs in water was recorded and analyzed

158 by the PIV system. The PSDs at different phases of the process were therefore obtained.

159 The inter-particle bonds that hold aggregate flocs together are considered as the

160 cohesive strength of the flocs. A size ratio method [20] is used here with an index (σ) to

161 express the strength of particle flocs, i.e.,

162 $$\sigma = d_2 / d_1 \tag{1}$$

163 where d_1 and d_2 are the mean sizes of the flocs before and after the shear breakage,

164 respectively. A higher value of the σ index indicates a higher strength of the flocs to resist

165 breakage when exposed to an elevated fluid shear.

166 When the shear intensity was reduced after the breakage phase, re-flocculation of the

167 particles could take place. A reversibility factor is used here to measure the re-flocculation

168 potential of the particles when the shear is reinstalled to its original level. A modified size

169 ratio approach may be applied to calculate the reversibility (γ) by

170 $$\gamma = \frac{d_3 - d_2}{d_1 - d_2} \tag{2}$$

171 where d_3 is the mean size of the particle flocs after re-flocculation at the original shear rate. A

172 higher reversibility index suggests a greater flocculation and re-growth capability of the flocs

173 after the shear breakage.

174

175 **3. Results and Discussion**

176

177 *3.1 Coagulation performance and water treatment results*

178 *3.1.1 ξ-potentials of the kaolin particles at different flocculant doses*

179 The clean kaolin was negatively charged with an average ζ-potential of around -30

180 mV (Figure 2). The presence of HA apparently increased the intensity of negative charges on

181   the particles, and the ζ-potential became more negative to -46 mV or below. Hence, HA

182   would cause further stabilization of particles in water. This is likely due to the steric or elastic

183   repulsion between particles brought about by the humic substances [21-23]. As anticipated,

184   addition of the flocculants, alum or ferric, could effectively reduce the surface charge of the

185   particles in all types of the model waters, resulting in particle destabilization. As the

186   flocculant dose increased, the particle ζ-potentials in the model waters approached zero.

187   Further increase in flocculant dose caused a certain extent of charge reversal of the particles

188   (Figure 2).

189   For pure kaolin with no HA in water, a small amount of the flocculants (5 mg/L or

190   lower) would eliminate the ζ-potentials and destabilize the particles completely. As the HA

191   content increased, the amount of alum or ferric required to achieve the same level of ζ-

192   potential reduction increased considerably. In comparison, alum appeared to be more

193   effective than ferric for reducing the ζ-potential of kaolin particles (Figure 2). For example,

194   with alum flocculation, the dose to neutralize the surface charge of kaolin was about 20 mg/L

195   for the HA3 water and 30 mg/L for the HA10 water. In ferric chloride flocculation, the

196   corresponding dose for charge neutralization was around 25 mg/L for HA3 and 30 mg/L for

197   HA10.

198

199   *3.1.2 Jar-test results of the flocculation and turbidity removal*

200   The jar-test flocculation and sedimentation results for turbidity and HA removals

201   from the model waters were in general agreement with would be expected from the ζ-

202   potential analysis. For clean kaolin without HA, a low flocculant dose of 5 mg/L was

203   sufficient to bring about flocculation for turbidity removal (Figure 3). With the presence of

204   HA in water, the flocculant demand for particle flocculation and turbidity removal increased

205   significantly. Alum appeared to be slightly more effective than ferric chloride for particle

206 flocculation. Nonetheless, a low alum dose below 20 mg/L still left a high level of HA

207 residue in water after flocculation and sedimentation. For the HA10 water with a high HA

208 content, at least 20 mg/L of alum or 25 mg/L of ferric chloride was needed to have

209 satisfactory flocculation and turbidity removal.

210   Enhanced flocculation with a high flocculant dose was effective to remove humic

211 substances from water (Figure 3). However, further increase of alum beyond 40 mg/L did not

212 bring about a notable improvement in turbidity and HA removals. For ferric chloride

213 flocculation, a dose of more than 40 mg/L actually worsened kaolin flocculation, particularly

214 for the HA0 and HA3 waters, resulting in poor turbidity removal. Judging from the ζ-

215 potential changes and jar-test results, the optimal alum doses chosen for the PIV-flocculation

216 experiments on the HA0, HA3 and HA10 waters were 10, 20 and 30 mg/L at pH~7.0,

217 respectively, and the optimal ferric chloride doses were 10, 25, and 30 mg/L at pH~6.5,

218 respectively.

219

220 *3.2 PSD dynamics, floc strength and re-flocculation capability*

221 *3.2.1 PIV characterisation of the flocculation dynamics*

222   The PIV technique is shown to be a powerful tool for obtaining the particle size

223 distributions in a dynamic fluid system. The PIV is a true non-intrusive particle tracking

224 system that is able to perform real-time *in-situ* particle imaging acquisition for determination

225 of the PSD dynamics during shear flocculation. The PSD of the flocs was expressed as the

226 volume-based discrete PSD, i.e. the percentages of the total particle volume observed against

227 a series of size sections (Figure 4).

228   The PIV results showed the continuous floc formation and growth in the model waters

229 during the chemical flocculation process. The PSD maintained a constant unimodal shape

230 with an apparent peak. Accordingly, the peak size, the particle size section corresponding to

231 the peak of the PSD curve, was used here as the mean size of the particle population observed

232 by the PIV. The change in the peak size of PSD with time illustrated well the flocculation-

233 breakage dynamics for a particle system. For both alum and ferric flocculation at the

234 respective optimal doses, flocs were well formed with a peak size of 1000 μm or larger. The

235 PSDs became rather stable in shape and position by the end of 30 min slow flocculation at 30

236 rpm. Shear breakage at a high stirring rate (100 rpm) caused a rapid and remarkable shift of

237 the PSDs to smaller sizes, and re-flocculation took place when the fluid shear was reduced

238 (Figure 4).

239 The PSD evolution showed effective alum and ferric flocculation on the jar-test

240 device (Figure 4). For either one of the flocculants, the HA0 water with pure kaolin and no

241 HA had the largest flocs formed, followed by the HA3 water and then the HA10 water. The

242 humic substances in water reduced the effectiveness of the flocculants in forming larger flocs.

243 However, with the higher doses used for HA3 and HA10 than that for HA0, floc formation in

244 the HA3 and HA10 waters occurred at a faster rate in the early phase of flocculation than that

245 in the HA0 water. In comparison, flocculation by alum produced larger flocs than ferric

246 chloride for the same water samples (Table 1). Nonetheless, compared to alum, ferric

247 chloride flocculation took place more rapidly after the chemical addition. For both

248 flocculants, the growth of particle flocs became much slower approaching the end of 30 min

249 slow flocculation.

250

251 *3.2.2 Breakage of the flocs and their re-flocculation*

252 A sudden increase in shear rate in the jar-test led to dramatic breakage of the

253 aggregate flocs in all water samples. Within 1 min or so, the peak sizes of the PSDs were

254 more than halved, according to the PIV observations (Figure 5). In agreement with previous

255 findings [19, 24], the large alum or ferric flocs formed by slow flocculation were rather

256   fragile and vulnerable to shear breakage. After the initial break-up, the breakage of the flocs

257   became much slower in the later phase of the breakage step. Thus, as suggested by others

258   [25-27], a shear breakage process may be classified into two phases. In the first phase, rapid

259   fragmentation of the flocs was the dominant phenomenon. In the following phase, particle

260   erosion could be the main cause for the slower decrease of floc sizes. Between the two

261   flocculants, ferric flocs appeared to be broken more easily to smaller flocs than alum flocs

262   (Figure 5).

263   As the shear was reduced to the original level, re-flocculation of the particles took

264   place, but to different extents in different model waters. Alum flocs were seen to have

265   considerable re-growth in size by flocculation (Figure 5). In comparison, ferric flocs were

266   more difficult to be recovered after breakage. The HA0 water showed the highest level of re-

267   flocculation for both flocculants, followed by HA3 and HA10. The humic matter in flocs

268   apparently decreased their potential of aggregation. In general, re-flocculation of the broken

269   particle flocs was a much slower process than the original flocculation after the flocculant

270   addition. Meanwhile, except for the alum flocs in HA0, the flocs recovered by re-flocculation

271   were much smaller in size than the flocs before breakage.

272

273   *3.2.3 Strength and recoverability of the alum and ferric flocs*

274   Based on the change in peak size of the PSD, the strength and reversibility of the

275   particle flocs formed in different model waters were determined (Table 1). After 15 min of

276   shear breakage, the alum flocs in HA0 showed the highest strength index at 32%. Other types

277   of flocs, including the alum flocs in HA3 and HA10 and all of ferric flocs had the strength

278   indexes that were rather similar to each other. In re-flocculation at a slower shear rate, the

279   alum flocs after breakage generally had a higher potential of recovery than the ferric flocs.

280   Pure kaolin flocs formed by alum flocculation had a of recovery index of 46%. As the HA

13

281   content in water increased, the recovery indexes of the broken flocs decreased significantly.

282   The alum flocs in HA10 had a low reversibility of only 10%. In agreement with the PIV

283   observations, the ferric flocs in HA10 after breakage almost could not be re-flocculated with

284   a recovery index as low as 4%.

285

286   *3.3 Morphology and Fractal Dimension of the Flocs*

287   *3.3.1 Morphology and boundary fractal dimension of the flocs*

288   The high-quality PIV images (Figure 6) also allow detailed analysis of the

289   morphology and structural features of the flocs suspended in water. According to equation 3,

290   the boundary fractal dimension of the particle flocs can be approximated from the slope of

291   the log-log regression of a series of projected areas versus perimeters of the particles. The D_b

292   of the flocs ranged from 1.11 to 1.22 after 30 min of slow flocculation (Figure 7). This is

293   somewhat lower than the value of from 1.1 to 1.4 reported for the aggregates of polystyrene

294   spheres [19]. For alum flocculation, flocs in the HA3 and HA10 waters had a slightly higher

295   D_b than that in HA0. For ferric chloride flocculation, flocs in HA10 had the highest D_b,

296   followed by HA3 and then HA0.

297   A higher D_b normally indicates a more irregular and/or elongated shape and a rougher

298   surface for the particles, whilst a lower D_b suggests a more spherical shape and a smoother

299   surface of the particles. Based on the D_b values, the flocs formed in the HA0 water at a low

300   alum or ferric chloride dose were less fractal with a more regular shape and smooth surface.

301   In comparison, the alum and ferric flocs formed by enhanced flocculation at higher flocculant

302   doses were more fractal with an elongated shape and a rougher surface.

303

304   *3.3.2 Change of the floc morphology during breakage and re-flocculation*

14

305   After the shear breakage, flocs in all of the model waters were smaller and became

306   less fractal in shape with reduced D_b values (Figure 7). When exposed to a higher shear, it is

307   expected that the flocs would break at their weak points and rearrange into more stable

308   structures [11, 28]. Fragmentation of the elongated flocs would break up the flocs into

309   smaller pieces that were more close to spherical objects than the original flocs. As described

310   previously, re-flocculation at a reduced shear rate resulted in regrowth of the floc sizes.

311   Meanwhile, the fractal structure of the particle flocs was recovered partially as indicated by

312   an increase in fractal dimension. Nonetheless, similar to the PSDs, the D_b of the flocs could

313   not be fully recovered to their original levels (Figure 7). After re-flocculation, the D_b values

314   of the alum flocs generally were somewhat higher than those of the ferric flocs, which was in

315   agreement with the indication of the recovery index of the broken flocs (Table 1).

316

317   *3.3.3 Effect of the humic content on particle flocculation and floc strength.*

318   The addition of chemical coagulants would impose mainly two aspects of impact on

319   particle flocculation in water. One effect is to destabilize particles in a suspension, which

320   enhances particle flocculation. The other effect is to form hydrolyzing metal salts and their

321   precipitates that adsorb particle colloids. [23, 29] pointed out that flocs formed following

322   charge neutralization should have a high recoverability after breakage. In comparison, the

323   precipitates of hydrolyzed flocculants would have a much lower recoverability after breakage

324   [24, 30]. In the HA0 water with pure kaolin and no HA, the low dose of the coagulants could

325   destabilize kaolin in the suspension by charge neutralization prior to particle flocculation.

326   Nonetheless, the partially reversible breakage of the HA0 flocs suggests that the formation of

327   the hydrolyzed flocculant precipitates and the adsorption of kaolin by the flocs of the

328   precipitates also played an important role in removing particulate turbidity from water. For

329   the HA3 and HA10 waters, more flocculants had to be used for kaolin adsorption and

330 removal. At a high flocculant dose, larger flocs of the precipitates would be formed more

331 easily. In agreement with previous findings [24, 30], these types of the flocs of hydrolyzed

332 precipitates in HA3 and HA10 waters had a lower recoverability after breakage compared to

333 the HA0 flocs (Table 1).

334   The content of organic matter appeared to be an important factor to determine the

335 surface properties of formed flocs, such as adhesion, inter-particle interaction and floc

336 stability [9, 31-32]. The HA content also affects the surface fractal dimension of the particle

337 flocs [33]. In this study, the HA presence apparently facilitated the formation of a more

338 porous and more fractal structure corresponding with a higher D_b (Figure 7). These results are

339 well consistent with the findings of [33]. They found that untreated kaolin formed flocs with

340 a less fractal and more regular structure and the flos of kaolin with HA attained a more

341 irregular and more fractal structure.

342

343 **4. Conclusion**

344   A series of standard jar-test flocculation experiments were performed on the model

345 waters with kaolin and various amounts of humic acids, 0 (HA0), 3 mg/L (HA3) and 10 mg/L

346 (HA10). Judging from the ζ-potential changes and the jar-test results, the optimal alum doses

347 for the HA0, HA3 and HA10 waters were 10, 20 and 30 mg/L, respectively, and the optimal

348 ferric chloride doses were 10, 25, and 30 mg/L, respectively.

349   The PIV technique was employed successfully to record and characterize the PSD

350 dynamics during the flocculation process in water treatment. The PIV system together with

351 the image analysis technique is capable to track the change in PSD on a jar-test during

352 particle flocculation and floc breakage and re-flocculation. Based on the change in the peak

353 size of the PSD, the strength and reversibility of the particle flocs formed in different model

354 waters were determined. The results showed that the alum flocs were somewhat stronger than

355 the ferric flocs. As the HA content in water increased, the recovery index of the flocs after

356 breakage decreased significantly. The alum flocs in HA10 had a reversibility of only 10%,

357 while the ferric flocs in HA10 after breakage could hardly be re-flocculated with a recovery

358 index as low as 4%.

359   According to the PIV images, the flocs formed initially after the flocculant addition

360 were larger and more fractal with a higher value of boundary fractal dimension D_b. After

361 shear breakage, the flocs became smaller and less fractal with a lower D_b. With the re-

362 flocculation, the fractal structure of the flocs could be only partially recovered. The results

363 suggested that initially aggregates have a ramified, open structure that became more compact

364 as exposure to a higher shear. An increase in floc compaction would lead to a reduction in

365 floc size, which provides a further explanation for the limited regrowth of most flocs. The

366 broken flocs seemed to become somehow difficult to form previous porous and fractal

367 clusters. It indicated the chemical bonds or/and chemical adsorption formed in first

368 aggregation phase were broken and flocs become more stable and rearrange into more

369 compact structure during the recovery stage.

370

376

377 **References**

378 [1] S. Chang, R.A. Berner, Humic substance formation via the oxidative weathering of coal.

379 Environ. Sci. Technol. 32 (1998) 2883-2886.

380 [2] W.P. Cheng, F.H. Chi, A study of coagulation mechanisms of polyferric sulfate reacting

381   with humic acid using a fluorescence-quenching method. Water Res. 36 (2002) 4583-

382   4591.

383 [3] A. Thekkedath, W.M. Naceur, K. Kecili, M. Sbai, A. Elana, L. Auret, H. Suty, C.

384   Machinal, M. Pontie, Macroscopic and microscopic characterizations of a cellulosic

385   ultrafiltration (UF) membrane fouled by a humic acid cake deposit: First step for

386   intensification of reverse osmosis (RO) pre-treatments. C. R. Chimie 10 (2007) 803-812.

387 [4] A. Rubia, M. Rodriguez, V.M. Leon, D. Prats, Removal of natural organic matter and

388   THM formation potential by ultra- and nanofiltration of surface water. Water Res. 42

389   (2008) 714-722.

390 [5] EPA, Enhanced coagulation and enhanced precipitative softening guidance manual. EPA

391   815-R-99-012, 1999.

392 [6] J.K. Edzwald, Enhanced coagulation: US requirements and a broader view. Water Sci.

393   Technol. 40 (1999) 63-70.

394 [7] D. Schmitt, H.E. Taylor, G.R. Aiken, D.A. Roth, F.H. Frimmel, Influence of natural

395   organic matter on the adsorption of metal ions onto clay minerals. Environ. Sci. Technol.

396   36 (2002) 2932-2938.

397 [8] Y. Wang, B. Du, J. Liu, B. Shi, H. Tang, Surface analysis of cryofixation-vacuum-

398   freeze-dried polyaluminum chloride–humic acid (PACl–HA) flocs. J. Colloid Interface

399   Sci. 316 (2007) 457-466.

400 [9] X. Y. Li, U. Passow, B. E. Logan, Fractal dimension of small (15-200 μm) particles in

401   Eastern Pacific coastal waters. Deep-Sea Res. 45 (1998) 115-118.

402 [10]N.D. Vassileva, van den D. Ende, F. Mugele, J. Mellema, Fragmentation and erosion of

403   two-dimensional aggregates in shear flow. Langmuir 23 (2007) 2352-2361.

404 [11] P.T. Spicer, S.E. Pratsinis, J. Raper, R. Amal, G. Bushell, G. Messters, The reversibility
405   of floc breakage. Powder Technol. 97 (1998) 26-34.

406 [12] V. Oles, Shear-induced aggregation and breakage of polystyrene latex particles. J.
407   Colloid Interf. Sci. 154 (1992) 351-358.

408 [13] K. A. Kusters, S. E. Pratsinis, S. G. Thoma, D. M. Smith, Ultrasonic fragmentation of
409   agglomerate powders. Chem. Eng. Sci. 48 (1993) 4119-4127.

410 [14] T. Serra, X. Casamitjana, Structure of the aggregates during the process of aggregation
411   and breakup under a sheer flow. J. Colloid Interface Sci. 206 (1998) 505-511.

412 [15] P. Meakin, Fractal aggreages. Adv Colloid Interface Sci. 28 (1988) 249-331.

413 [16] Q. Jiang, B.E. Logan, Fractal dimensions of aggregates determined from steady-state size
414   distributions. Environ. Sci. Technol. 25 (1991) 2031-2038.

415 [17] S.R. Grey, C.B. Ritchie, T. Tran, B.A. Bolto, Effect of NOM characteristics and
416   membrane type on microfiltration performance. Water Res. 41 (2007) 3833-3841.

417 [18] M. Raffel, C.E. Willert, J. Kompenhans, Particle image velocimetry: a practical guide.
418   Springer, Berlin, 1998

419 [19] P.T. Spicer, S.E. Pratsinis, Coagulation and fragmentation: Universal steady-state
420   particle-size distribution. AIChE J. 42 (1996) 1612-1620.

421 [20] P. Jarvis, B. Jefferson, J. Gregory, S.A. Parsons, A review of floc strength and breakage.
422   Water Res. 39 (2005) 3121-3137.

423 [21] M. Elimelech, J. Gregory, X. Jia, R. A. Williams, Particle deposition and aggregation:
424   measurement, modelling and simulation, Butterworth-Heinemann, Woburn, MA, 1995.
425   p9−63, 261−289.

426 [22] M. Stumm, J.J. Morgan, Aquatic Chemistry: Chemical Equilibrium and Rates in Natural
427   Waters. Wiley, New York, 1995.

428   [23] A. Amirtharajah, C.R. O'Melia, Coagulation processes: Destabilisation, Mixing and

429   Flocculation. In AWWA Water Quality and Treatment: a Handbook of Community

430   Suppliers. McGraw-Hill, New York, 1999.

431   [24] R.J. Francois, Ageing of aluminum hydroxide flocs. Water Res. 21 (1987) 523-531

432   [25] D.S. Parker, W.J. Kaufman, D. Jenkins, Floc breakup in turbulent flocculation processes.

433   Journal of the Sanitary Engineering Division-ASCE 98 (NSA1) (1976) 79-99.

434   [26] P.A. Shamlou, S. Stavrinides, N. Titchener-hooker M. Hoare, Growth-independent

435   breakage frequency of protein precipitates in turbulently agitated bioreactors. Chem.

436   Eng. Sci. 49 (1994) 2647-2656.

437   [27] C.A. Biggs, P.A. Lant, Activated sludge flocculation: On-line determination of floc size

438   and the effect of shear. Water Res. 34 (2000) 2542-2550.

439   [28] C. Selomulya, R. Amal, G. Bushell, T.D. Waite, Evidence of shear rate dependence on

440   restructuring and break-up of latex aggregates. J. Colloid Interface Sci. 236 (2001) 67-

441   77.

442   [29] V. Chaignon, B.S. Lartiges, A.El. Samrani, C. Mustin, Evolution of size distribution and

443   transfer of mineral particles between flocs in activated sludges: an insight into floc

444   exchange dynamics. Water Res. 36 (2002) 676-684.

445   [30] K. McCurdy, K. Carlson, D. Gregory, Floc morphology and cyclic shearing recovery:

446   comparison of alum and polyaluminum chloride coagulants. Water Res. 38 (2004) 486-

447   494.

448   [31] M.R. Jekel, The stabilization of dispersed mineral particles by adsorption of humic

449   substances. Water. Res. 20 (1996) 1543 – 1554.

450   [32] B. Janczuk, T. Białopiotrowicz, A. Zdziennicka, M. Hajnos, G. Jozefaciuk, The influence

451   of soil clay constituents on surface free energy of clay fractions. J. Soil Sci. 43 (1992)

452   27–35.

453 [33]Z. Sokolowska, S. Sokolowski, Influence of humic acid on surface fractal dimension of

454 kaolin: analysis of mercury porosimetry and water vapour adsoption data. Geodema 88

455 (1998) 233-249.

456

457 **Figure captions**

458 Figure 1. Schematic diagram of the PIV coupling with an image analysis system.

459 Figure 2. ζ-potential of the three particle systems as a function of the coagulant dose.

460 Figure 3. Turbidity and TOC after the jar-test flocculation and sedimentation experiments as

461   a function of the flocculant dose for the three particle systems.

462 Figure 4. PSD profiles of the particles flocs for different HA contents in water during the A-

463   B-R process.

464 Figure 5. Change of the peak size of flocs for different HA contents in water during the A-B-

465   R tests.

466 Figure 6. Examples of the PIV images of particle flocs during a typical A-B-R process.

467 Figure 7. Change of the fractal dimension of the particle flocs with different HA contents in

468   water during the A-B-R tests.
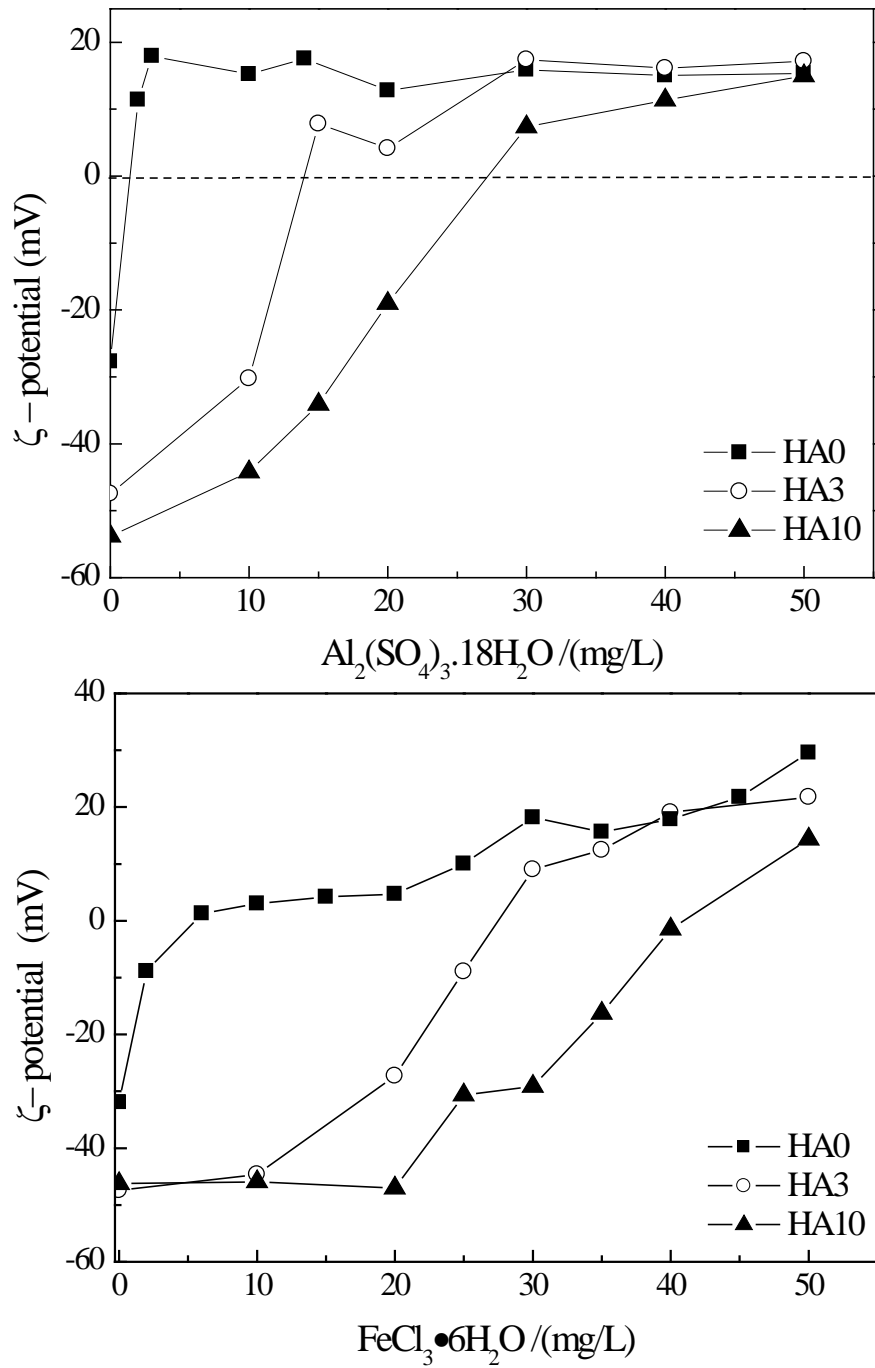
469

470

471

472
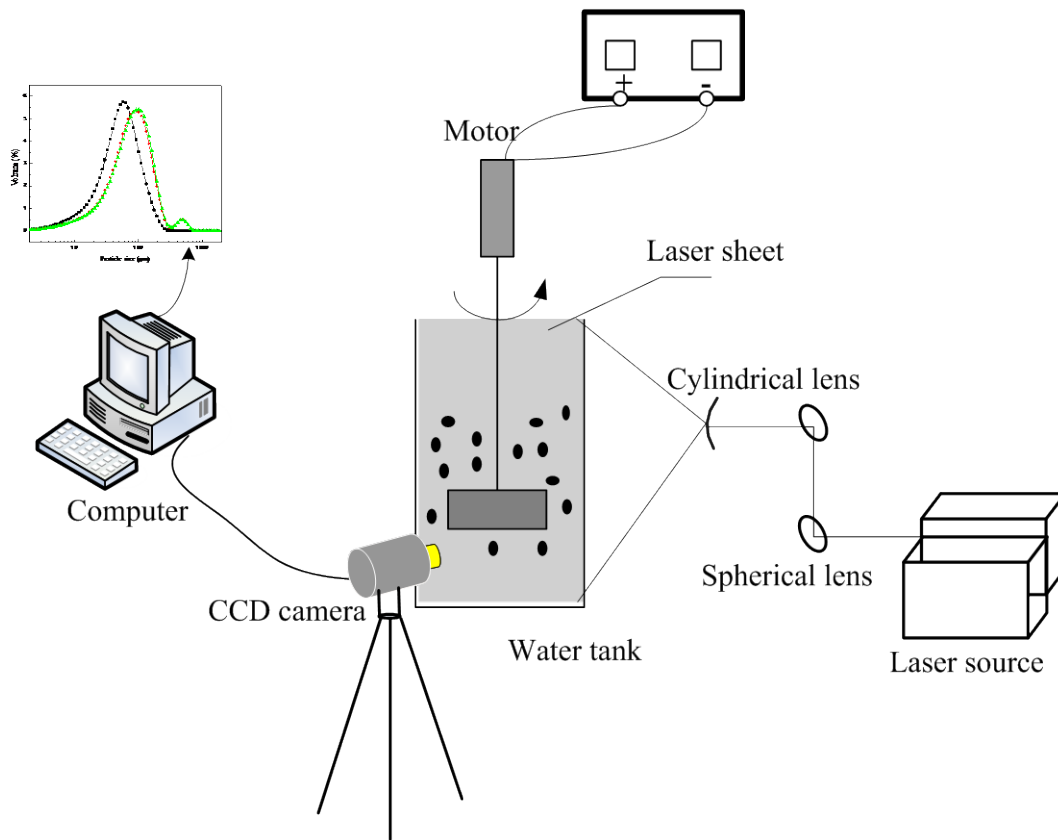
473

474

475   **Figure 1.** Schematic diagram of the PIV coupling with an image analysis system.
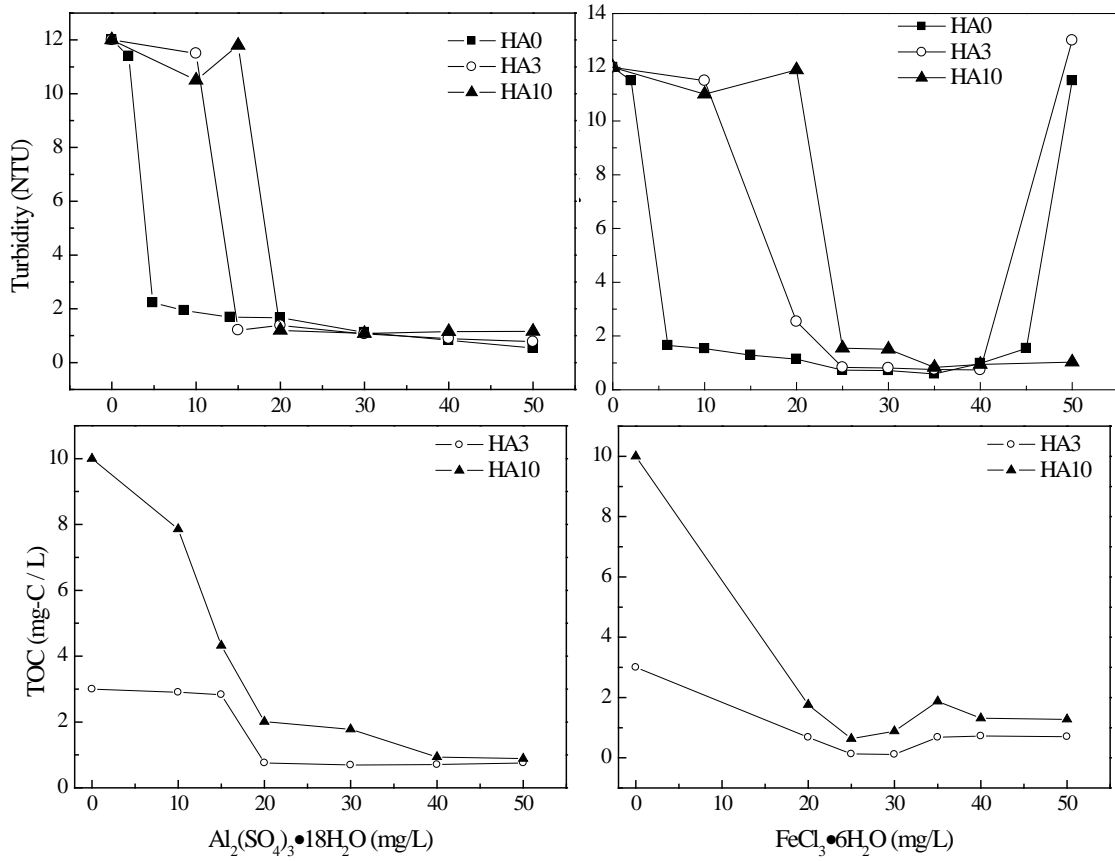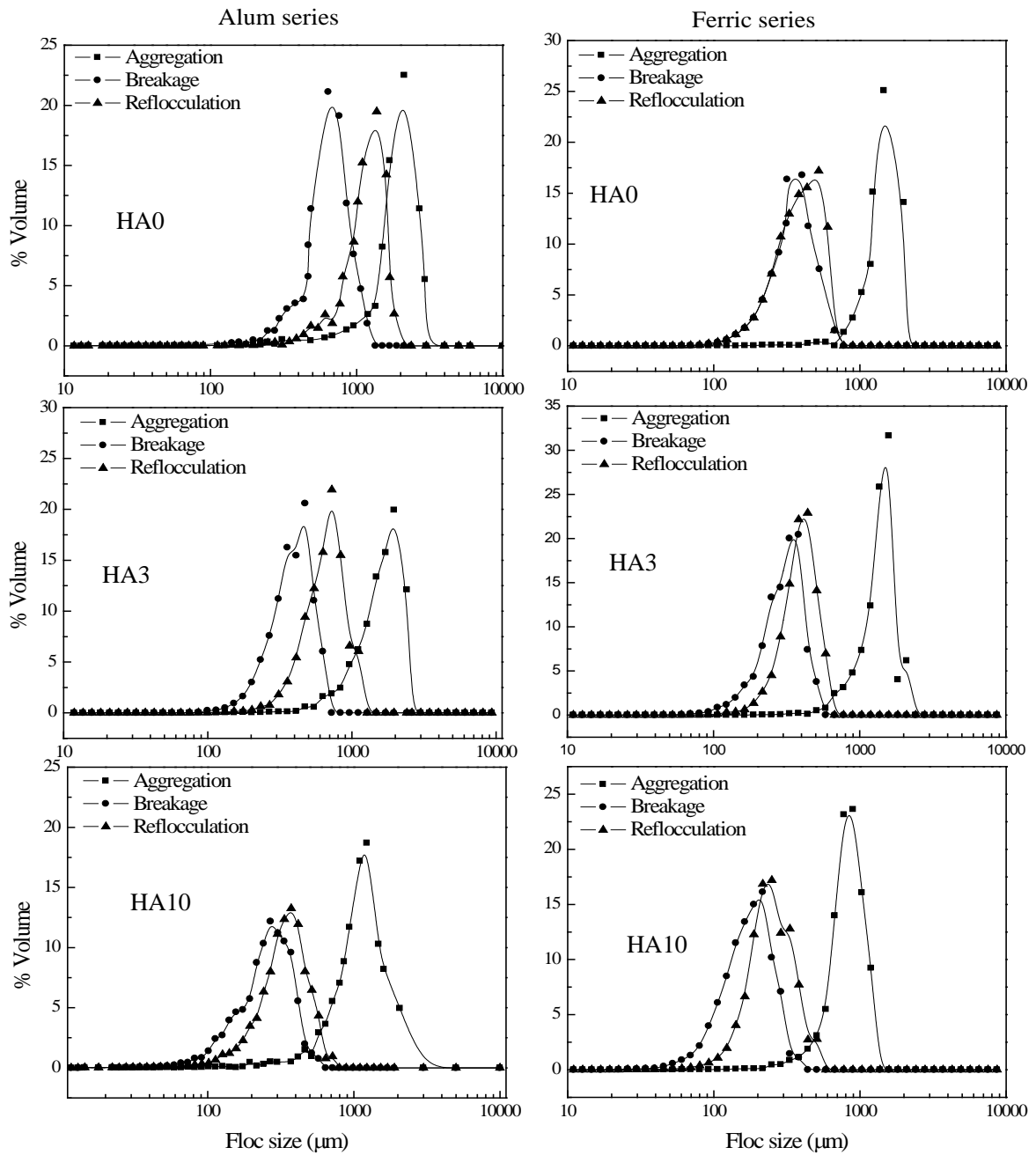
476

477

Figure 2. ζ-potential of the three particle systems as a function of the coagulant dose.

479

480

481

482

483

Figure 3. Turbidity and TOC after the jar-test flocculation and sedimentation experiments as
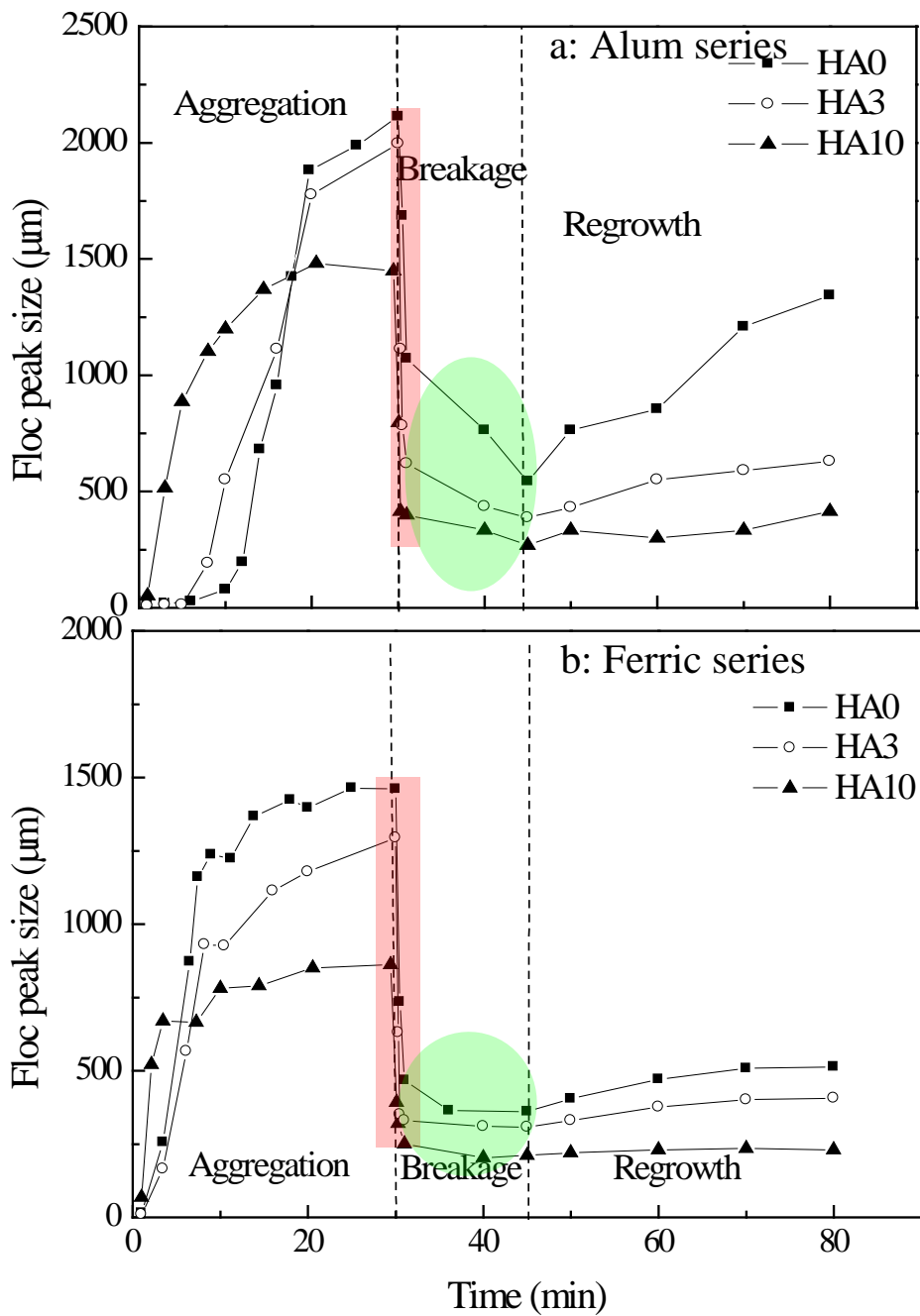a function of the flocculant dose for the three particle systems.

486

487

490

Figure 4. PSD profiles of the particles flocs for different HA contents in water during the A-
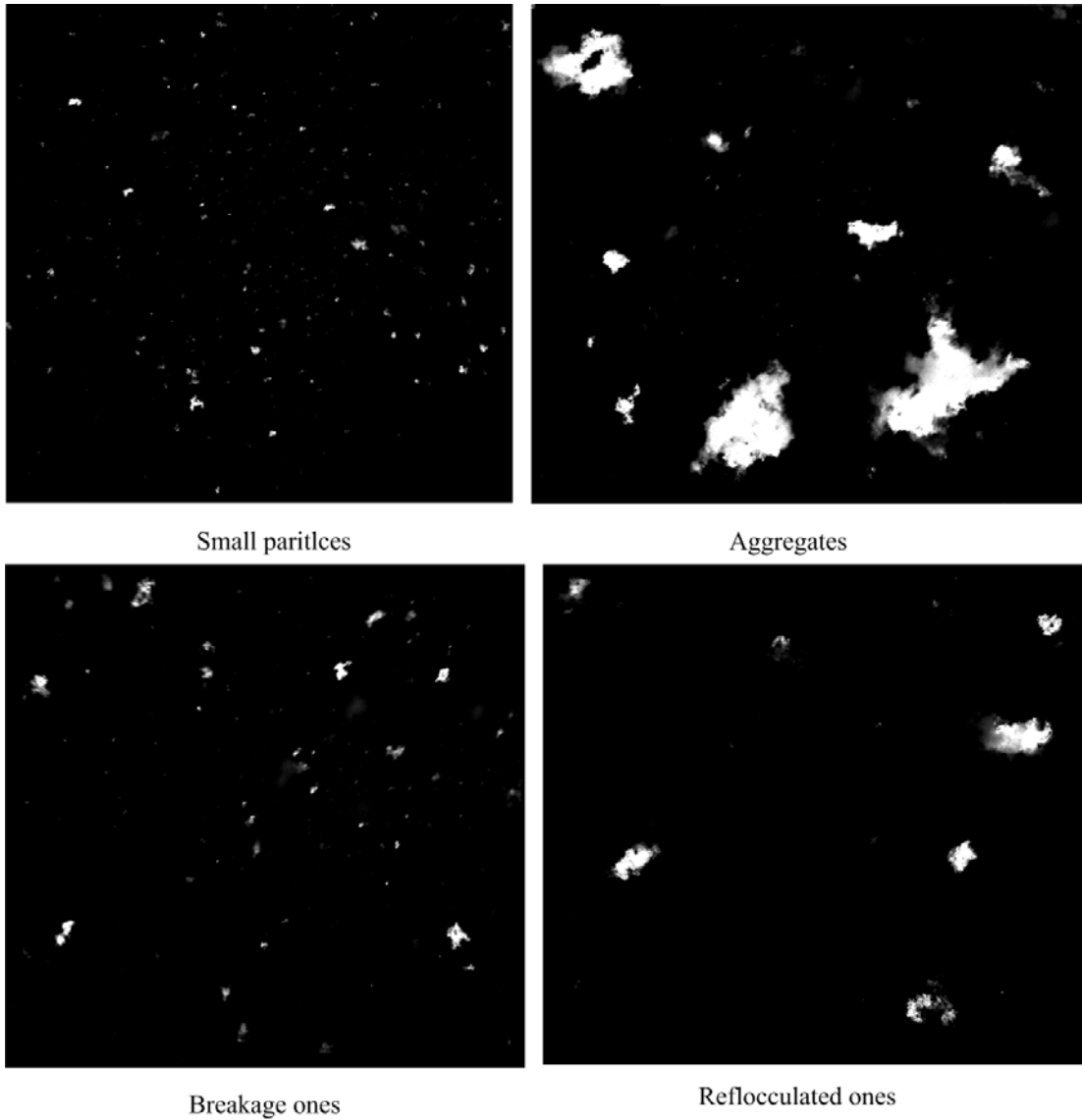
B-R process.

493

494

495

496

Figure 5. Change of the peak size of flocs for different HA contents in water during the A-B-R tests.
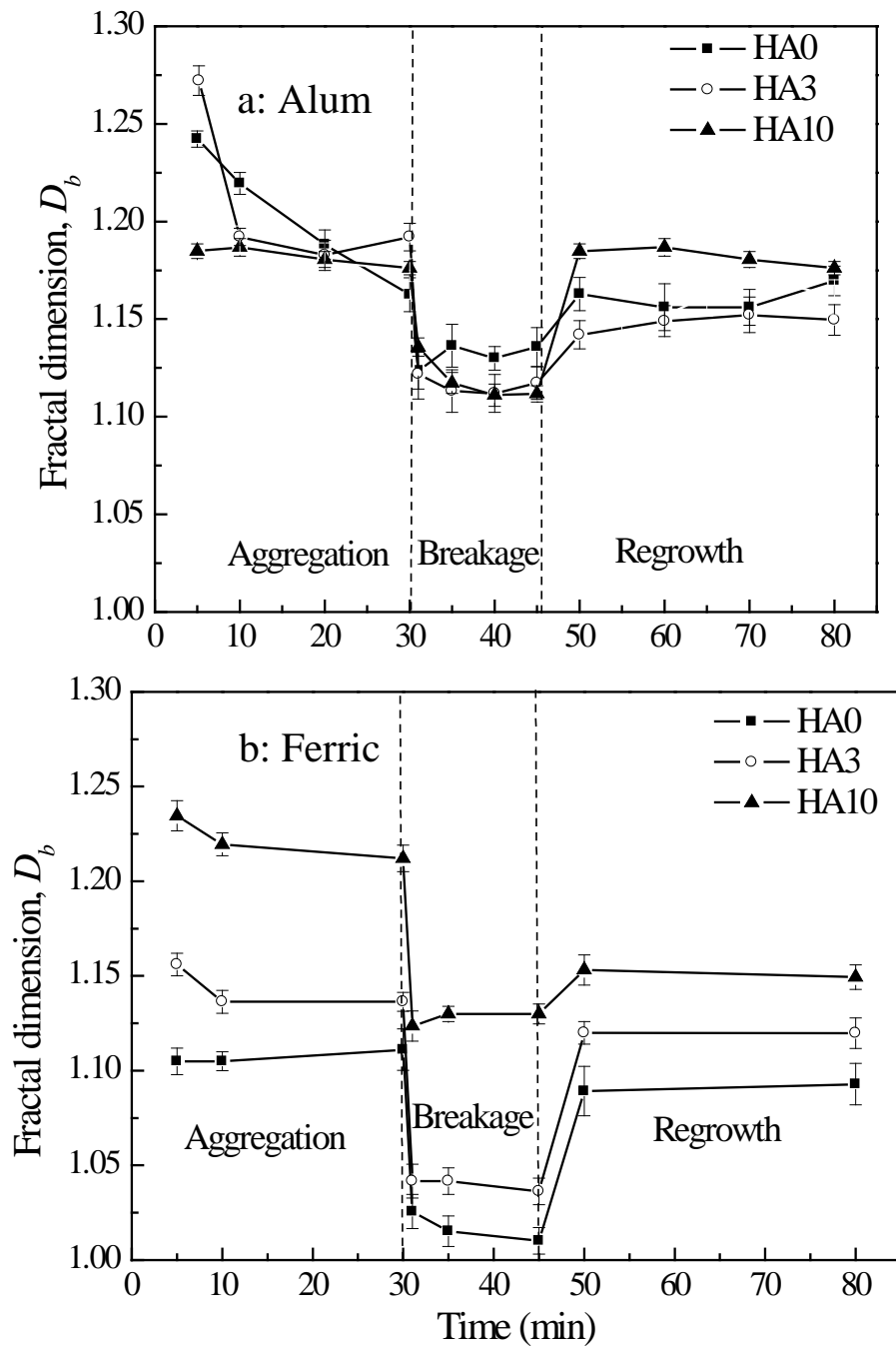
499

500

501

502

Small paritlces

Aggregates

Breakage ones

Reflocculated ones

Figure 6. Examples of the PIV images of particle flocs during a typical A-B-R process.

509

510

511   **Figure 7**. Change of the fractal dimension of the particle flocs with different HA contents in

512   water during the A-B-R tests.